Journal of Rock Mechanics and Geotechnical Engineering 7 (2015) 226–232

Contents lists available at ScienceDirect

Journal of Rock Mechanics and Geotechnical Engineering

journal homepage: www.rockgeotech.org

Full length article

Liquefaction evaluation of dam foundation soils considering overlying structure

Gang Wang [a,*], Xing Wei [b], Hanlong Liu [a]

[a] School of Civil Engineering, Chongqing University, Chongqing 400044, China
[b] School of Civil Engineering, Southwest Jiaotong University, Chengdu 610031, China

ARTICLE INFO

Article history:
Received 9 December 2014
Received in revised form
4 February 2015
Accepted 5 February 2015
Available online 25 February 2015

Keywords:
Liquefaction
Overlying structure
Dam
Stone columns

ABSTRACT

The liquefaction analysis procedure conducted at a dam foundation associated with a layer of liquefiable sand is presented. In this case, the effects of the overlying dam and an embedded diaphragm wall on liquefaction potential of foundation soils are considered. The analysis follows the stress-based approach which compares the earthquake-induced cyclic stresses with the cyclic resistance of the soil, and the cyclic resistance of the sand under complex stress condition is the key issue. Comprehensive laboratory monotonic and cyclic triaxial tests are conducted to evaluate the static characteristics, dynamic characteristics and the cyclic resistance against liquefaction of the foundation soils. The distribution of the factor of safety considering liquefaction is given. It is found that the zones beneath the dam edges and near the upstream of the diaphragm wall are more susceptible to liquefaction than in free field, whereas the zone beneath the center of the dam is less susceptible to liquefaction than in free field. According to the results, the strategies of ground improvement are proposed to mitigate the liquefaction hazards.

1. Introduction

Based on empirical correlations of some observed performance of "liquefaction/non-liquefaction" case histories, several simplified approaches employing in situ test indices have been developed for assessing liquefaction potential of soils (Seed and Idriss, 1971; Seed, 1979). These simplified approaches can only be used to evaluate liquefaction triggering for level or nearly level free field ground without structures. While in practice these simplified approaches were widely used to evaluate the liquefaction potential of soils beneath or near a structure, the soils beneath a structure are treated as if they are in the free field under level ground conditions and the effect of the buildings resting on the ground surface is ignored.

Field case histories, model tests and numerical analysis suggested that conditions influencing liquefaction near a structure may be substantially different from those for the same soil profile in the free field. Although the influence of structures on potential liquefaction damage has not been well understood, the following conclusions can be drawn (Liu and Qiao, 1984; Rollins and Seed, 1990; Cetin et al., 2012). (1) The excess pore water pressure distribution near a building can be much different from that in the free field. (2) The liquefaction potential of soil may be greater or lesser beneath a structure, depending mainly on the structure type and soil density. For instance, sands underneath low-rise and short-period structures appear to have higher liquefaction potential, while sands underneath tall and long-period structures appear to have lower liquefaction potential than in the free-field. (3) The ground under the edges of a structure is more susceptible to triggering liquefaction than that under the center of the structure. Some modifications were suggested for the free-field liquefaction evaluation procedure to account for the structure effects. Men et al. (1998) proposed a simple method to evaluate dynamic stress of the ground exerted by aboveground structures, and developed a simplified method to evaluate liquefaction of building's subsoils. Jing et al. (2001) further considered the subsoil's nonlinearity in the framework of the method proposed by Men et al. (1998). Yang et al. (2010) adopted an equivalent influence depth to consider additional stress exerted by a finite building base, and revised the standard penetration test (SPT)-based method adopted by Chinese code GB 50287–2008 (MOHURD, 2008). Noorzad et al. (2009) evaluated the effect of structures on the wave-induced liquefaction potential of seabed by applying a structure force on the underlying sand deposits. Based on numerical results of generic soils, structure and earthquake combinations, Cetin et al. (2012) developed an alternative simplified procedure for three-dimensional

* Corresponding author. Tel.: +86 13808216151.
E-mail address: cewanggang@163.com (G. Wang).
Peer review under responsibility of Institute of Rock and Soil Mechanics, Chinese Academy of Sciences.
1674-7755
http://dx.doi.org/10.1016/j.jrmge.2015.02.005

(3D) dynamic response assessment of soil and structure systems, which can produce unbiased estimates of the representative and maximum soil–structure–earthquake-induced cyclic stress ratio values. Meanwhile, Oka et al. (2012) considered the effect of heavy structures on the liquefaction potential of the foundation soils by incorporation of mean stresses in the framework of the simplified procedure.

Although some advances have been made on seismic liquefaction assessment of foundation soils beneath structures, to consider the effect of overlying structures on liquefaction evaluation still remains a controversial and difficult issue. The effect of structures on the liquefaction potential of foundation soils depends on both the characteristics of structures and soils, so direct applicability of the simplified methods (e.g. Seed–Idriss procedure or Chinese simplified procedure) to foundation soils beneath structures is impossible, unless the soil–structure–earthquake interaction is reliably addressed in the estimation of cyclic stress ratio (CSR) (Cetin et al., 2012). Numerical method can not only consider almost all the factors influencing the interaction between structures and subsoils but also be an efficient way to solve this problem. The key problem in numerical method is the criterion for judging liquefaction triggering in complex stress conditions. To illustrate these trivial but essential matters in the numerical method, the liquefaction analysis procedure of a practical case, a dam built on the foundation with a liquefiable sand layer, is presented. The procedure includes two aspects: (1) detailed field exploration and comprehensive laboratory tests to determine the criterion for liquefaction triggering of the sand layer, and (2) 3D finite element analysis to calculate the static and dynamic interaction between the dam and underlying soils.

It should be noted that some exciting progress has been achieved in the aspects of constitutive modeling of sand and the codes for fully coupled dynamic response analysis of saturated porous media (Wang and Zhang, 2007; Wang et al., 2011; Zhang and Wang, 2012). The whole liquefaction process, including the onset of liquefaction, the process of generation, diffusion and release of excess pore water pressure, and even the development of liquefaction-induced deformation, can be simulated by the fully coupled dynamic numerical methods. The whole liquefaction process simulation involves comprehensive constitutive models with complicated codes of fully coupled dynamic consolidation and large amount of testing work (e.g. Zhang and Wang, 2012). As a result, it is not very appealing and sometimes impractical for small engineering projects. The procedure adopted in this study intends to overcome these issues, so that it would be efficient and economical for middle or small projects.

2. A sluice dam in China

A typical sluice dam in China is taken as an example to illustrate the procedure for liquefaction assessment. This type of dam is not very high, and natural deposits are usually taken as the foundation. As shown in Fig. 1, the dam is composed of four sluice segments in the middle of the river and two gravity dam segments located at the left and right abutments, respectively. The sluice segments are 27.5 m in height. The alluvial deposits underlying the sluice segments are from 35 m to 47 m in depth. The deposits are composed of 3 layers. The soils from top to bottom are gravel, sand and gravel, respectively. The sand layer is 5–10 m in thickness, and is distributed all over the dam site.

The content of the particle size less than 5 mm of the sand layer is greater than 70% and the fine particle content is less than 13%, therefore the sand is classified as fine sand. The maximum and minimum dry densities of the sand layer are 1.72 g/cm^3 and 1.28 g/cm^3, respectively. The specific gravity G_s of the sand is 2.72. Site exploration reveals that the relative density of the intact sand layer is around 50%. The designed earthquake intensity of the dam is VII degree (corresponding peak ground acceleration is about 100 cm/s^2). According to GB 50287–2008 (MOHURD, 2008), the sand layer is preliminary judged to be susceptible to liquefaction. Further judgment of liquefaction triggering is based on the blow counts of SPT proposed by GB 50287–2008 (MOHURD, 2008). The in situ SPT blow counts $N'_{63.5}$ is about 8–9. Considering that the operation conditions of the sluice dam are different from the test conditions, the in situ SPT blow counts $N'_{63.5}$ should be corrected, which is something like the surcharge pressure correction in Seed's simplified procedure, and the corrected average SPT blow counts $N_{63.5}$ is 6.7. According to GB 50287–2008 (MOHURD, 2008), the critical SPT blow counts N_{cr} for triggering liquefaction is 7.5 for earthquake intensity VII, so the liquefaction would be triggered in the sand layer under the earthquake of intensity VII.

3. Numerical procedure for liquefaction evaluation

The stress-based approach compares the earthquake-induced CSR with the cyclic resistance ratio (CRR) of the soil to judge whether liquefaction would be triggered. The factor of safety (FS) against the triggering of liquefaction can then be computed as the ratio of the sand's CRR to the earthquake-induced CSR:

$$FS = CRR/CSR \tag{1}$$

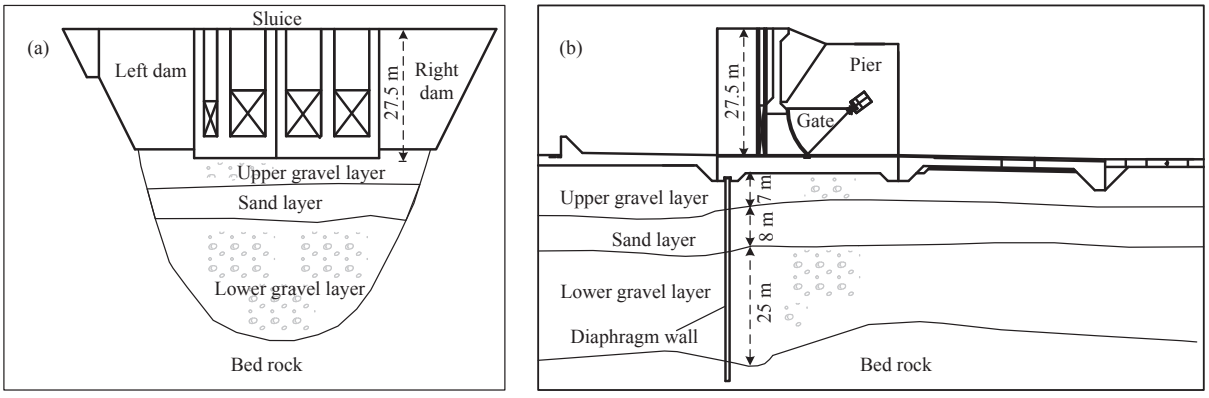

Fig. 1. Geological profile of the dam foundation. (a) Longitudinal section, and (b) Transverse section.

$$CSR = 0.65\tau_{max}/\sigma'_{v0} \quad (2)$$

where τ_{max} is the peak value of horizontal shear stress, and σ'_{v0} is the vertical effective consolidation stress. The time history of earthquake-induced cyclic stress involves numerous irregular cycles of different amplitudes. Various studies showed that an irregular time history can be approximated by a uniform cyclic stress time history with an equivalent number of uniform cycles depending on the uniform cyclic stress amplitude. Commonly, a representative value (or equivalent uniform value) equal to 65% of the peak cyclic stress is adopted as the amplitude of the equivalent uniform cyclic stress series.

3.1. Estimating earthquake-induced CSR

The earthquake-induced CSR can be estimated via the Seed–Idriss simplified procedure (Seed and Idriss, 1971) or numerical methods such as finite element method (FEM)-based seismic response analysis. Seed–Idriss simplified procedure can only be used to estimate the earthquake-induced cyclic stresses beneath level ground sites without structures subjected primarily to horizontal shaking. In this case, there exists a dam overlying on the surface of the ground and a diaphragm wall embedded in the foundation soil, so at least two factors would alter the CSR of the underground deposits induced by earthquake shaking. The two factors are the change in vertical effective stress induced by the dam load and the influence of response interaction between the dam and the subsoils. In addition to these factors, a two-step analysis procedure is adopted. Firstly, a static analysis is conducted to obtain the initial static stress before earthquake. The process of the dam construction and reservoir filling are modeled. And then, specified earthquake acceleration time history is input to the FEM model to obtain the dynamic stresses of the foundation soils.

In static stress analysis, Duncan and Chang (1970)'s model is adopted for constitutive description of foundation soils. Four monotonic triaxial drained compression tests are conducted to determinate the parameters of Duncan and Chang's model, in which isotropically consolidated undrained (ICU) samples are adopted with initial confining pressure σ_{3c} of 100 kPa, 200 kPa, 400 kPa and 800 kPa, respectively. The height and the diameter of the sand samples are 8 cm and 3.8 cm, respectively. The samples have a relative density of 50% (i.e. an initial dry density of 1.47 g/cm^3) and are saturated by vacuum method. The model parameters for foundation soils determined by these triaxial tests are shown in Table 1.

The dynamic response analysis is based on the technology of equivalent linear procedures. The nonlinear cyclic stress–strain characteristics are approximated by an equivalent modulus G/G_{max} and damping ratio λ, where G is the dynamic shear modulus and G_{max} is the maximum dynamic shear modulus. Because G/G_{max} and λ vary with the amplitude of the cyclic shear strain γ, two groups of resonant column tests are conducted to determine the relationship between G/G_{max} and λ changing with shear strain of the sand layer, in which anisotropically consolidated undrained (ACU) sample with stress ratio $\sigma_{1c}/\sigma_{3c} = 2.0$ and two levels of confining pressure σ_{3c} (100 kPa and 400 kPa) are adopted, where σ_{1c} is the axial consolidation stress. The confining pressure and the stress ratio are selected according to the range of the in situ static stress before and after the construction of the dam. The sand specimens in resonant column tests have a height of 10 cm, a diameter of 5 cm and a relative density D_r of 50%. According to the results of resonant column tests, the maximum dynamic shear modulus of the sand can be determined by mean effective stress as $G_{max} = 800(p/p_a)^{0.5}$, where p is the mean effective stress and p_a is the atmospheric pressure (=101 kPa). The resonant column tests also present the relationship of dynamic shear modulus ratio and damping ratio changing with dynamic shear strain, as shown in Fig. 2. In the analysis, the values of shear modulus and damping ratio are determined by iterations so that they become consistent with the level of shear strain induced in each element.

Table 1
Duncan and Chang model's parameters of foundation soils.

Layer	ρ (g cm^{-3})	c (kPa)	φ (°)	K	n	R_f	K_b	m
Upper gravel	2.35	0	43	850	0.42	0.82	380	0.25
Sand	2.15	0	33	133	0.75	0.79	43	0.42
Lower gravel	2.37	0	46	950	0.44	0.78	405	0.3

Note: ρ is the density of the soil, c and φ are the Mohr–Coulomb shear strength parameters, K is the Young's modulus coefficient, n is the exponent determining the rate of variation of the Young's modulus with confining stress, R_f is the failure stress ratio, K_b is the bulk modulus coefficient, and m is an exponent determining the rate of variation of the bulk modulus with confining stress.

3.2. Evaluating CRR of sand

There are mainly two approaches to estimate the CRR of saturated sands. One approach is testing the specimens in cyclic laboratory tests and the other is through semi-empirical correlations between in situ CRR and the in situ test indices. Although the in situ tests widely used to evaluate liquefaction characteristics include SPT, cone penetration test (CPT), back pressure test (BPT), large penetrometer test (LPT), and shear wave velocity (V_s) test, these correlations between CRR and in situ test indices are developed mainly based on the case histories of the free-field, level ground conditions. In this case, inside the foundation soils, there exist initial static shear stresses on horizontal planes, and the confining pressures and over-consolidation ratio are changed due to the overlying dam. For these reasons, the CRR of the soils beneath or near the dam could be different from the CRR of the soils under the free-field, level ground conditions. So the CRR estimated by the semi-empirical correlations based on in situ test indices should be corrected accordingly.

Laboratory cyclic triaxial tests under undrained conditions are conducted to estimate the CRR of the sand layer. Two levels of effective confining stress (200 kPa and 500 kPa) are adopted in the tests to reflect the effect of confining stress level on the CRR. The selected confining stress level can roughly cover the field confining stress of the sand before and after dam construction plus the additional effect of earthquake. Both ICU samples and ACU samples are tested to reflect the effect of a static shear stress on cyclic behaviors of sand. The samples have a height of 8 cm, a diameter of 3.8 cm, and an initial relative density of 50%. Fig. 3 shows the results

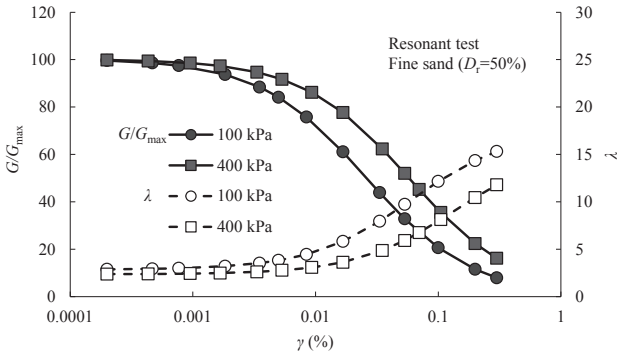

Fig. 2. The change of modulus and damping ratio of the sand with shear strain.

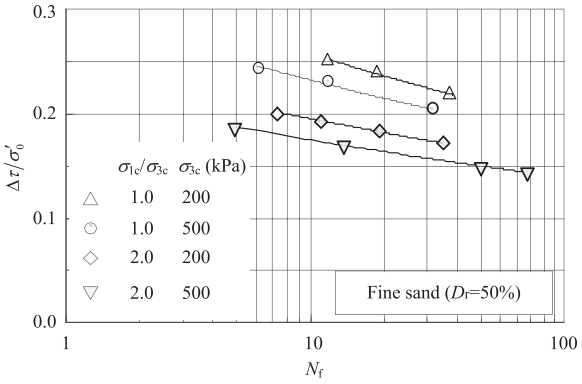

Fig. 3. Cyclic resistance of the sand vs. number of cycles.

of the cyclic triaxial tests. In Fig. 3, N_f is the number of loading cycles, $\Delta\tau/\sigma'_0$ is the cyclic stress ratio required to reach liquefaction in a specified loading cycles, $\Delta\tau = \Delta\sigma_1/2$ is the cyclic shear stress in 45° plane of specimens, $\sigma'_0 = (\sigma_{1c} + \sigma_{3c})/2$ is the initial effective normal stress in 45° plane of specimens, and $\Delta\sigma_1$ is cyclic axial stress.

Due to the differences in consolidation stress state between cyclic triaxial tests and field conditions, the CRR measured in cyclic triaxial tests should be corrected for field conditions as follows (Ishihara et al., 1985):

$$CRR_{field} = 0.9\left(\frac{1+2K_{0,field}}{3}\right)CRR_{tx} \tag{3}$$

$$K_{0,field} = \sigma'_{hc}/\sigma'_{vc} \tag{4}$$

where $K_{0,field}$ is the field consolidation ratio, σ'_{hc} is the horizontal effective confining stress, and σ'_{vc} is the vertical effective confining stress. The coefficient 0.9 in Eq. (3) is a reduction coefficient considering two-directional simple shear loading in field as suggested by Seed (1979).

The effect of a static shear stress on the CRR of sand depends on initial static shear stress ratio, relative density, confining stress, etc. Different initial consolidation stress ratios in triaxial tests result in different magnitudes of static shear stress on the 45° plane of the specimen. Fig. 3 shows the CRR at two different confining stresses and two different consolidation stress ratios. The consolidation stress ratio can be converted to the initial static shear stress ratio on the 45° plane. In the analysis, the CRR of each element of soil is determined by interpolation in the results (see Fig. 3) according to the initial consolidation stress and initial static shear stress ratio of the element.

3.3. CSR of sand in composite foundations

The method of vibro-replacement stone columns was proposed to improve the liquefiable sand layer. The improved foundation is composed of stone columns and the sand. In the FEM analysis, the composite foundation is assumed homogeneous. Based on the principle of deformation consistency, the modulus of the composite foundation E_{sp} can be approximated by the following formula, as suggested by GB 50007–2002 (MOHURD, 2002):

$$E_{sp} = [1 + \overline{m}(\overline{n} - 1)]E_s = \xi E_s \tag{5}$$

where $\overline{m}$ is the area replacement ratio of stone columns, $\overline{n}$ is the stress ratio of stone columns to the in situ sand, E_s is the modulus of the in situ sand, and ξ can be regarded as the reinforcement coefficient of the composite foundation compared to the natural foundation. For sand ground, after improved by vibro-replacement stone columns, GB 50007–2002 (MOHURD, 2002) suggested that the stress ratio $\overline{n}$ of stone columns to the sand can be supposed to be about 1.5–3. The lower the modulus of the sand is, the higher the value of $\overline{n}$ is. After improvement by stone columns, the vertical stress induced by the overlying dam and the cyclic shear stresses induced by earthquake loading would have an apparent reduction. This effect would also lead to an apparent decrease in liquefaction potential of the sand layer. When the cyclic shear stresses of the composite foundation τ_{sp} induced by earthquake are calculated by FEM analysis, the cyclic shear stress of the sand τ_s can be deduced from Eq. (5) as

$$\tau_s = \frac{\tau_{sp}}{1 + \overline{m}(\overline{n} - 1)} = \frac{\tau_{sp}}{\xi} \tag{6}$$

That is to say, the stress of the sand is the stress of the composite foundation divided by the reinforcement coefficient. Because the consolidation process of the soil deposit under gravity-driven load has completed, the initial geostatic stress of the soil is kept in the sand. The dam is constructed after the foundation improvement, so the additional vertical stress of the sand due to the dam load should be reduced. Consequently, the cyclic stress ratio of the sand layer (CSR_s) can be calculated as

$$CSR_s = \frac{\tau_{sp}}{\xi\sigma_{vs,0} + (\sigma_{v,sp} - \sigma_{vs,0})} \tag{7}$$

where $\sigma_{v,sp}$ is the effective vertical stress of the composite foundation, and $\sigma_{vs,0}$ is the initial effective vertical stress of the natural soil deposits before dam construction.

4. Results and discussion

4.1. FEM model

The 3D discretized meshes of the sluice dam and foundation are illustrated in Fig. 4. Three stages are simulated in static analysis: (1) the diaphragm wall completed; (2) the dam and sluice completed; and (3) reservoir filling to normal pool level. The stress condition at stage 3 is assumed as the initial stress condition for seismic response analysis. According to the earthquake risk assessment report issued by China Earthquake Administration (CEA), the seismic precautionary intensity at the dam site is VII degree, and the peak acceleration at base rock surface is 106 cm/s^2. The input earthquake wave is shown in Fig. 5, which is artificially generated by CEA with the predominant period of the input earthquake of about 0.2 s. According to the *Specifications for Seismic Design of Hydraulic Structures* (DL 5073–2000) (IWHR, 2000), the basic designed seismic intensity of the dam is equal to the seismic precautionary intensity at the dam site (i.e. VII), and the dam design should be checked in accordance with earthquake intensity of VIII, which have a peak acceleration of about 219 cm/s^2 given by CEA.

4.2. Initial conditions before earthquake

Fig. 6 shows the static stresses distribution on middle horizontal plane of the sand layer. In Fig. 6, σ'_x is the normal stress along the dam axis direction, σ'_y is the normal stress along river flow direction, σ'_z is the vertical stress, τ_{yz} is the shear stress along river flow direction, and the red dotted lines show the boundary of the sluice. The calculated shear stress along dam axis direction is relatively small, so it is not plotted. The vertical stress σ'_z is apparently concentrated near the dam. And because the diaphragm wall is pushed downstream by the water load, σ'_z in the upstream of the

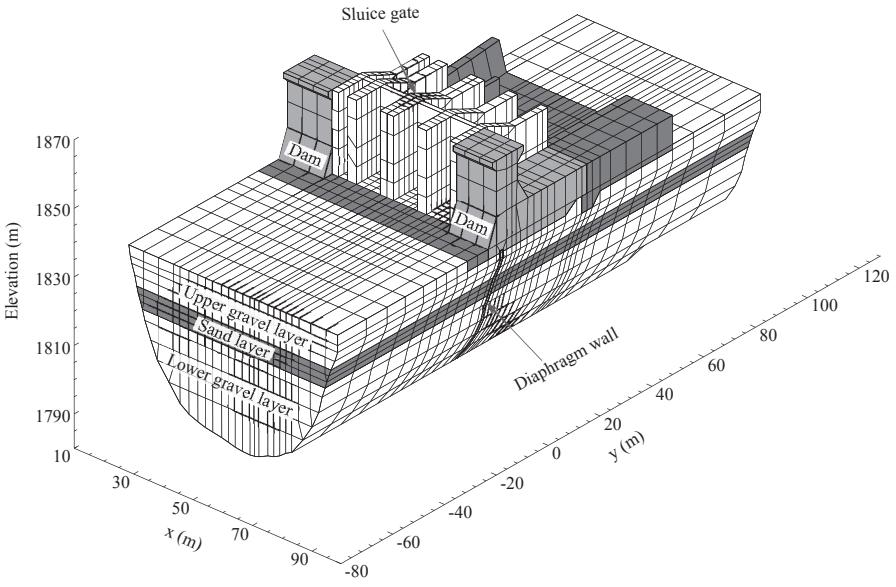

Fig. 4. 3D finite element mesh of dam and foundation.

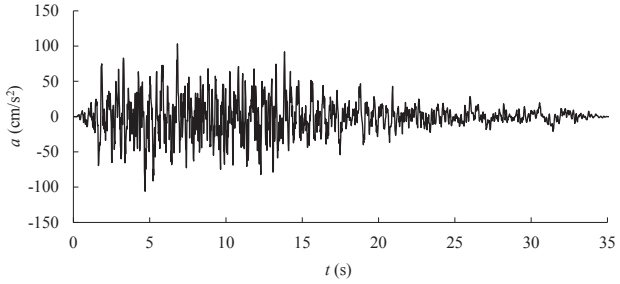

Fig. 5. Input earthquake wave (intensity VII).

wall is much less than that in the downstream. The shear stress τ_{yz} is also concentrated near the diaphragm wall, and that in the downstream side of the sluice gate is apparently larger than in other zones. In presence of the overlying structure, the static stress distribution beneath and near the dam is significantly different from that in the free field. Due to the influence of the diaphragm wall, the stress distribution in the foundation soil is much more sophisticated. Mere corrections of the simplified method for the level free-field ground cannot reflect the effect of such complicated boundary conditions on the stress distribution of the foundation soils.

4.3. Cyclic stresses and liquefaction potential

Fig. 7 shows the cyclic stress time history of a typical element of sand subjected to an earthquake of intensity VII. According to Fig. 7, the time history of equivalent uniform cyclic stress of 65% peak cyclic stress with an equivalent number can be determined. The equivalent number of cycles mainly depends on earthquake magnitude. In this case, an earthquake magnitude of 7.5 with 15 equivalent cycles is assumed based on the empirical relationships

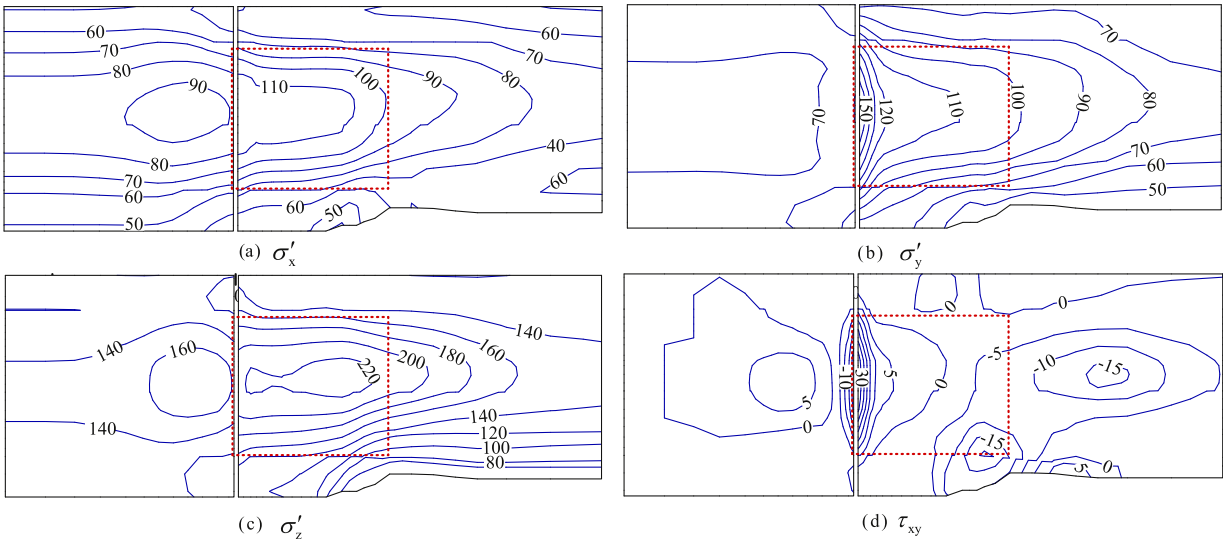

Fig. 6. The distribution of static stresses of the sand layer (unit: kPa).

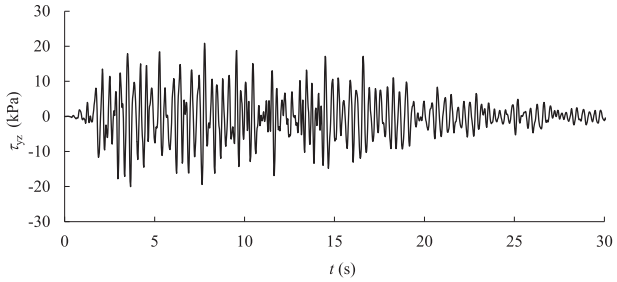

Fig. 7. Time history of cyclic shear stress of typical element in sand layer.

(Green and Terri, 2005). Fig. 8 presents the peak cyclic shear stress on the middle horizontal plane of the sand layer. The shear stress beneath and near the dam is obviously larger than that in other zones. Fig. 9 shows the distribution of the factor of safety against liquefaction on the middle plane of the sand layer. In the sand layer, the minimum value of the *FS* beneath the dam is about 1.25, but near the upstream and downstream edges of the dam the *FS* is less than 1.0, suggesting that the liquefaction would be triggered in this zone. In the edge of the dam vertical effective stress is relatively small and the cyclic shear stress induced by earthquake is relatively large, so in this region the CSR is large and exceeds the CRR. It should be also noticed from Fig. 8 that the horizontal normal stress of the sand near the upstream side of the diaphragm wall is small, so the liquefaction resistance in this area apparently decreases.

Furthermore, Fig. 10 presents the distribution of the factor of safety against liquefaction on the middle plane of the sand layer subjected to earthquake of intensity VIII. The peak acceleration of intensity VIII is about 219 cm/s^2. The minimum value of the factor of safety beneath the dam is only 0.7. Fig. 10 indicates that the sand layer in the overall dam site would trigger liquefaction when subjected to an earthquake of intensity VIII.

4.4. Suggestions for ground improvement

A simple criterion suggested practically by GB 50287–2008 (MOHURD, 2008) is also adopted. The criterion requires that the minimum value of the replacement ratio $\overline{m}$ should make the *N* value of the soil SPT between the stone columns N_{sp} equal to or greater than the critical *N* value for liquefaction N_{cr}, i.e. $N_{sp} \geq N_{cr}$. But according to the liquefaction analysis based on seismic response analysis, in the condition of intensity VII, only the sand near the upstream and downstream edges of the dam would liquefy, the sand beneath the center of the dam has a relatively high factor of safety against liquefaction.

In the condition of intensity VIII, if no liquefaction triggering is required, a larger area of foundation improvement is needed. Theoretically, the CSR reduction as presented in Section 3.3 in the foundation can be employed to evaluate the parameters for improvement. For example, assuming the stress ratio of stone

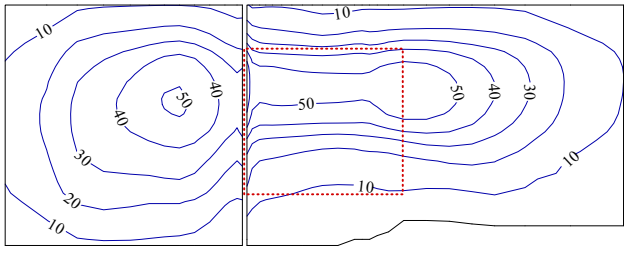

Fig. 8. Contours of peak shear stress of sand layer (unit: kPa).

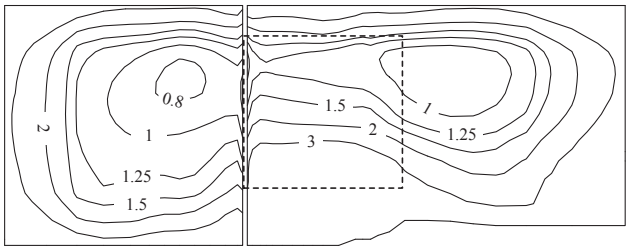

Fig. 9. Contours of factor of safety against liquefaction in sand layer (intensity VII).

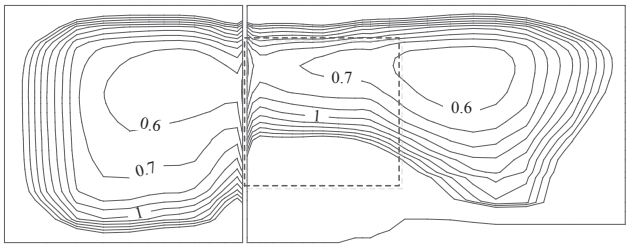

Fig. 10. Contours of factor of safety against liquefaction in sand layer (intensity VIII).

columns to sand $\overline{n}$ is 2, the replacement area ratio $\overline{m}$ may be taken as 0.2. In addition to reinforcing the soil mass, the vibro-replacement method can improve liquefiable soil deposits by (1) densifying the in situ soils, (2) increasing the in situ lateral stress, and (3) providing increased drainage of earthquake-induced excess pore water pressures. So in practical cases, a smaller value can be taken for the replacement area ratio according to empirical judgment.

By using the presented method, the distribution of the factor of safety against liquefaction can be given. Thus different design parameters for ground improvement can be assumed for different zones. For this project, the ground improvement should be focused on the upstream side of the diaphragm wall and the edges of the dam. The simplified method suggested by GB 50287–2008 (MOHURD, 2008) does not always produce conservative estimates of the liquefaction triggering response and it may miss the most susceptible regions.

5. Conclusions

Based on the stress criteria and seismic response analysis, the liquefaction potential of a liquefiable foundation overlying a sluice dam is evaluated. A 3D FEM model including the dam and foundation is established, thus both the static and dynamic interaction effects between the dam and foundation are considered in the calculated CSR of the foundation. The results show that (1) the soil near the edges of the dam is more prone to liquefy than that beneath the center of the dam, and (2) the simplified liquefaction evaluation procedure proposed by GB 50287–2008 (MOHURD, 2008) is conservative for the soil beneath the center of the dam, and unsafe for the soil near the edges of the dam. The procedure presented in this study can give the distribution of the safety factor against liquefaction, depending on site-specific boundary conditions. The foundation soil can be zoned according to the distribution of the factor of safety, so the countermeasures for ground improvement may be more efficient.

Liquefaction analysis of foundation soils of a building is much different from free-field ground, and must consider the interaction between building and subsoils. The liquefaction potential of the subsoils beneath a building depends on both the characteristics of

the building and the subsoils. The numerical method and codes involved in the present procedure are promising, and the amount of test works is acceptable for most engineering projects, thus the procedure can be suggested for most practical engineering problems. As stated above, the criterion for liquefaction triggering under complex stress conditions is the key problem of the present procedure, and it determines the reliability of the results. Therefore, the cyclic resistance of liquefiable soil should be carefully estimated through field investigation, laboratory tests and experiences.

Conflict of interest

The authors wish to confirm that there are no known conflicts of interest associated with this publication and there has been no significant financial support for this work that could have influenced its outcome.

Acknowledgments

The authors appreciate the support from the National Natural Science Foundation of China (No. 51209179).

References

Cetin K, Unutmaz B, Jeremic B. Assessment of seismic soil liquefaction triggering beneath building foundation systems. Soil Dynamics and Earthquake Engineering 2012;43:160–73.
China Institute of Water Resources and Hydropower Research (IWHR). Specifications for seismic design of hydraulic structures (DL 5073–2000). Beijing: China Electric Power Press; 2000 (in Chinese).
Duncan JM, Chang CY. Nonlinear analysis of stresses and strains in soils. Journal of Soil Mechanics and Foundation Division, ASCE 1970;96(5):1629–53.
Green RA, Terri GA. Number of equivalent cycles concept for liquefaction evaluations – revised. Journal of Geotechnical and Geoenvironmental Engineering, ASCE 2005;131(4):477–88.
Ishihara K, Yamazaki A, Haga K. Liquefaction of K_0-consolidated sand under cyclic rotation of principal stress direction with lateral constraint. Soils and Foundations 1985;5(4):63–74.
Jing LP, Chen WH, Ge LC. A simplified method for evaluating liquefaction of building's subsoil with consideration of nonlinear constitutive relationship. Earthquake Engineering and Engineering Vibration 2001;21(2):121–5 (in Chinese).
Liu H, Qiao T. Liquefaction potential of saturated sand deposits underlying foundation of structure. In: Proceedings of the 8th World Conference on Earthquake Engineering. San Francisco, USA: Prentice-Hall, Inc.; 1984. p. 199–206.
Men FL, Cui J, Jing LP, Chen WH. A simplified method to evaluate liquefaction of building's subsoil. Chinese Journal of Hydraulic Engineering 1998;29(5):33–8 (in Chinese).
Ministry of Housing and Urban-Rural Development of the People's Republic of China (MOHURD). Code for geological investigation of water resources and hydropower engineering (GB 50287–2008). Beijing: China Planning Press; 2008 (in Chinese).
Ministry of Housing and Urban-Rural Development of the People's Republic of China (MOHURD). Code for design of building foundation (GB 50007–2002). Beijing: China Architecture and Building Press; 2002 (in Chinese).
Noorzad R, Safari S, Omidvar M. The effect of structures on the wave-induced liquefaction potential of seabed sand deposits. Applied Ocean Research 2009;31(1):25–30.
Oka LG, Dewoolkar MM, Olson SM. Liquefaction assessment of cohesionless soils in the vicinity of large embankments. Soil Dynamics and Earthquake Engineering 2012;43:33–44.
Rollins KM, Seed HB. Influence of building on potential liquefaction damage. Journal of Geotechnical Engineering 1990;116(2):165–85.
Seed HB, Idriss IM. Simplified procedure for evaluating soil liquefaction potential. Journal of Soil Mechanics and Foundations Division, ASCE 1971;97(9):1249–73.
Seed HB. Soil liquefaction and cyclic mobility evaluation for level ground during earthquakes. Journal of Geotechnical Engineering Division, ASCE 1979;105(2):201–55.
Wang G, Zhang J, Wei X. Seismic response analysis of a subway station in liquefiable soil. Chinese Journal of Geotechnical Engineering 2011;33(10):1623–7 (in Chinese).
Wang G, Zhang J. Recent advances in seismic liquefaction research. Advances in Mechanics 2007;37(4):575–89 (in Chinese).
Yang Y, Liu X, Liu Q, Chen N. Study on the method for evaluating sand liquefaction potential. Chinese Journal of Hydraulic Engineering 2010;41(9):1061–8 (in Chinese).
Zhang J, Wang G. Large post-liquefaction deformation of sand, part I: physical mechanism, constitutive description and numerical algorithm. Acta Geotechnica 2012;7(2):69–113.

Dr. Gang Wang is working as a professor in School of Civil Engineering at Chongqing University, China. He worked as a senior engineer and deputy chief engineer in the Yalong River Hydropower Development Company (2005–2014). His research interests cover constitutive modeling of soils, geotechnical earthquake engineering, dam engineering, numerical methods in geotechnical engineering, etc.